ACS NANO

www.acsnano.org

ARTICLE

A Large-Area Transferable Wide Band Gap 2D Silicon Dioxide Layer

Christin Büchner, Zhu-Jun Wang, Kristen M. Burson, Marc-Georg Willinger, Markus Heyde,* Robert Schlögl, and Hans-Joachim Freund

Fritz-Haber-Institut der Max-Planck-Gesellschaft Faradayweg 4-6, 14195 Berlin, Germany

ABSTRACT: **An atomically smooth silica bilayer is transferred from the growth substrate to a new support *via* mechanical exfoliation at millimeter scale. The atomic structure and morphology are maintained perfectly throughout the process. A simple heating treatment results in complete removal of the transfer medium. Low-energy electron diffraction, Auger electron spectroscopy, scanning tunneling microscopy, and environmental scanning electron microscopy show the success of the transfer steps. Excellent chemical and thermal stability result from the absence of dangling bonds in the film structure. By adding this wide band gap oxide to the toolbox of 2D materials, possibilities for van der Waals heterostructures will be broadened significantly.**

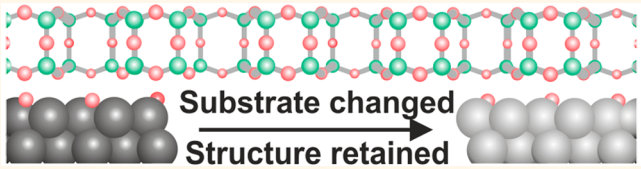

KEYWORDS: *2D materials, 2D silicon dioxide, dielectric, exfoliation, transfer, PMMA assisted*

While graphene remains the child prodigy of materials research, a whole class of two-dimensional structures is being explored, due to the fascinating changes in electronic and optical properties that are observed when going from bulk-thickness to surface-only compounds. It is only by combining conductors with semiconductors and insulators at the nanoscale that electronic device building can keep up with Moore's law of shrinking transistor size. Recently, a 2D silicon dioxide (also called silica) film was presented.[1,2] It is atomically flat and consists of amorphous and crystalline domains, structurally resolved with atomic resolution.[3,4] The metal-supported silica film has been thoroughly investigated theoretically and experimentally, revealing structure,[5] electronic properties,[6] and chemical behavior.[7−9] It is a promising candidate for an ultrathin dielectric in nanoelectronic devices, but has so far only been studied on its respective growth substrates. The ability to transfer a silica film from one substrate to another is a requirement for utilizing this building block in nanoarchitectures.

Figure 1 shows a schematic top view and side view for graphene and a boron nitride monolayer (ML) in comparison to the 2D silica layer (shown without substrate). The silicon dioxide film consists of a sandwich structure similar to transition metal dichalcogenides and can be described as a double-row of SiO_4 tetrahedra. This silica bilayer is the thinnest attainable layer with the stoichiometry SiO_2, as monolayers were found to have the stoichiometry $SiO_{2.5}$.[10] The bilayer system has so far been grown and investigated at the atomic scale on ruthenium,[2] platinum,[11] palladium,[12] cobalt,[13] and graphene on copper foils.[14] Each building block is a SiO_4 tetrahedron with three in-plane oxygen bridges and a fourth oxygen bridge linking to the second layer. Hence, all building units are coordinatively saturated, and no covalent bonds connect the bilayer with the underlying support. Only weak substrate interaction is expected, mostly based on van der Waals forces, which were estimated to be roughly equal to the interlayer forces in graphite.[1] This relatively weak adhesion indicates the possibility to remove the silica film from the growth substrate. The tetrahedral units can form rings of different sizes. Shown in the silica top view in Figure 1c is an amorphous silica sheet, where different ring sizes tile the plane without long-range order. It is important to note that the amorphous silica sheet remains atomically smooth in the *z*-direction, as shown in the side view, Figure 1f. Depending on growth conditions and substrate influence, silica bilayers can exhibit crystalline, amorphous, or coexisting structures.[15,16]

Due to its large band gap, bulk silica is universally applied for electrically insulating components. The dielectric properties of the 2D silica film complement conductive materials such as graphene in heterostructures.[17−19] The commonly observed reduction of carrier mobility in graphene supported on standard SiO_2 substrates in the form of oxidized wafer surfaces is often assigned to charged impurities and graphene corrugation induced by adhesion to the rough substrate.[20−25] The SiO_2 bilayer used in this transfer study is atomically smooth and charge neutral, making it a potential candidate for the dielectric spacer in ever-smaller transistors.[26,27] First scanning tunneling spectroscopy (STS) measurements of the band edge on the ruthenium-supported bilayer indicate a gap of 6.5 eV.[6] Freestanding silica bilayer structures were recently predicted (with DFT calculations using an HSE06 functional) to have band gaps of approximately 6.7−7.3 eV.[28] Thus, silica bilayers

Received: June 14, 2016
Accepted: July 15, 2016
Published: July 15, 2016

DOI: 10.1021/acsnano.6b03929
ACS Nano 2016, 10, 7982−7989

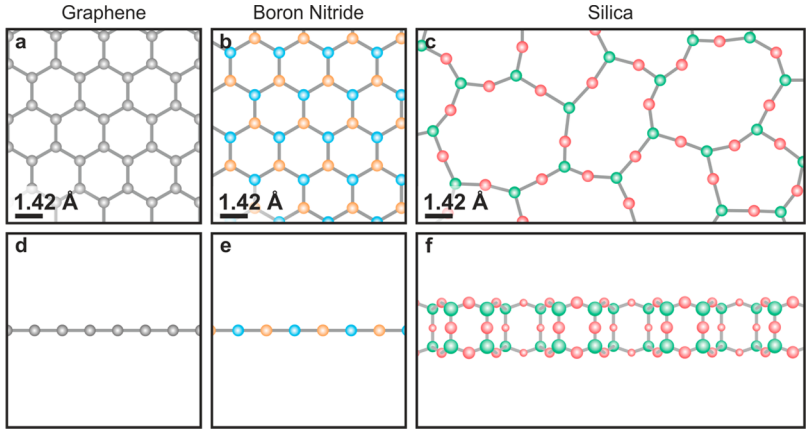

Figure 1. Comparison of graphene, boron nitride monolayer, and silica bilayer. Top view of (a) graphene, (b) boron nitride monolayer, and (c) silica bilayer. Scale bar shown for typical lateral bond lengths. Side view of (d) graphene, (e) boron nitride monolayer, and (f) silica bilayer.

present an alternative to h-BN monolayers, which until now are the most widely used 2D insulators, with a band gap of roughly 5.5 eV.[29−31]

Several other properties of this film have been investigated that render it a promising 2D material. Other oxide nanosheets are exfoliated from (polycrystalline) layered oxides, which yields sheets of variable thickness and lateral sizes of micrometers.[18] Silica bilayers grow epitaxially on centimeter-scale substrates, yielding an atomically defined, self-saturated film. Since the 2D silica film is charge neutral, no stabilization is needed from counterions or polar molecules. The bilayer film has been shown to be chemically inert and to hydroxylate only upon activation such as electron irradiation.[8,9,32] The amorphous network structure provides nanopores that are larger than those of graphene or boron nitride, which allows size-selective diffusion of small species through the film.[7,9,33,34] The lack of long-range order in the amorphous film also implies that the performance of silica bilayers in van der Waals stacks would not be limited by anisotropies in the lateral direction.

We present comprehensive experimental evidence for a successful transfer of an atomically smooth silica bilayer grown on Ru(0001) to a Pt(111) substrate. Preservation of the structure is shown with Auger electron spectroscopy (AES), low-energy electron diffraction (LEED), environmental scanning electron microscopy (ESEM), and scanning tunneling microscopy (STM) both on a large scale and with high resolution.

RESULTS

The 2D silicon dioxide films used in this study share characteristic features, which are highlighted in Figure 2. The ring features that are indicated in the schematic in Figure 1c are shown in an STM image with atomic resolution in Figure 2a. The experimental contrast shows the Si atoms from which the positions of O atoms were subsequently inferred.[2] An amorphous network pattern is visible, which is the dominant structure observed for this coverage regime. The occurrence of the different ring sizes is shown in the histogram plot (Figure 2b). This log-normal ring size distribution is typical for 2D amorphous networks.[35] A sub-bilayer coverage is deposited on the ruthenium substrates, which yields bilayer films with large holes (up to 30 nm in diameter, resolved with STM). This is shown schematically in Figure 2c and in a 40 × 40 nm^2 STM image in Figure 2d. Round holes in the flat film expose the

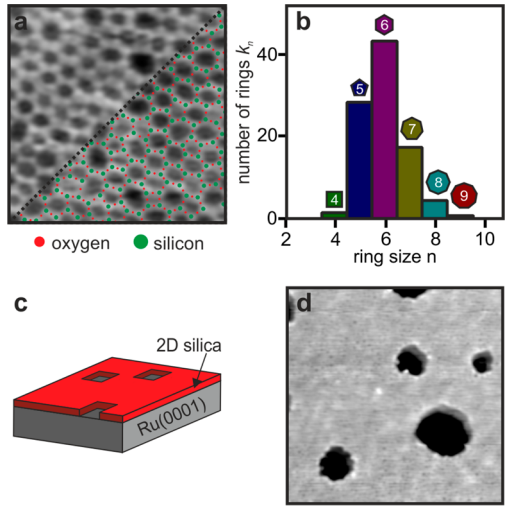

Figure 2. Typical features of the silica bilayer films used in this study. (a) Atomic resolution STM image of an amorphous silica bilayer on Ru(0001). Oxygen and silicon atomic positions are marked on the lower half of the image with red and green circles, respectively (5 nm × 5 nm, V_S = 1 V, I_T = 50 pA). (b) Ring size histogram of the amorphous network shown in panel a. (c) Schematic showing partial coverage of the silica bilayer. (d) Large-scale STM image showing partial coverage of the silica bilayer (overall coverage 1.8 ML) (40 nm × 40 nm, V_S = 3 V, I_T = 10 pA).

substrate. A coverage of 1.8 ML is assigned through quantitative analysis of the holes. Preparations ranging from 1.5 to 1.8 ML were used for transfers. Besides the holes visible in STM, on the flat film, nanoscale structures are also visible. The coverage and amorphous network structure presented here are representative of the samples used in this study. In the discussion we will comment on how these characteristics facilitate the success of the exfoliation in particular.

The transfer procedure is shown as a schematic in Figure 3 and consists of two main parts: the exfoliation of the film from the growth substrate (panels a−d) and the subsequent transfer to a new substrate of choice (panels e, f). A detailed description of each transfer step can be found in the Methods section. It should be noted that while the silica bilayer preparation was carried out in ultrahigh vacuum, the entire transfer can be carried out in ambient environment. The samples then were again transferred to ultrahigh vacuum (UHV) in order to use

DOI: 10.1021/acsnano.6b03929
ACS Nano 2016, 10, 7982−7989

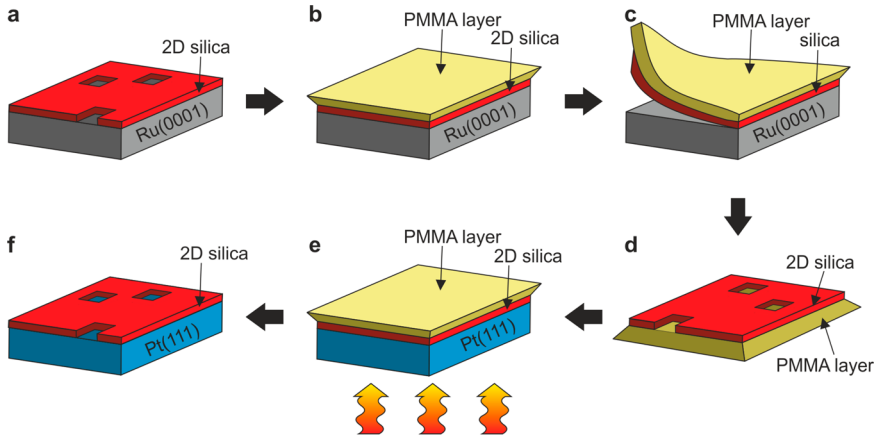

Figure 3. Schematic of the transfer procedure. (a) Silica bilayer on ruthenium substrate. (b) Spin coating of system with PMMA layer. (c) Mechanical exfoliation of PMMA; silica adheres to PMMA layer. (d) Silica supported on PMMA layer. (e) Placing the PMMA-supported silica layer on clean Pt(111) substrate, subsequent heat treatment. (f) After PMMA removal, silica is supported on Pt(111) substrate.

the surface science methods for sample analysis. All samples transferred from ambient to UHV were treated with a short heating step.

For the exfoliation, a silica bilayer film supported on a Ru(0001) substrate is spin-coated with poly(methyl methacrylate) (PMMA) dissolved in acetone, and the PMMA-supported silica film is removed from the ruthenium crystal by mechanical exfoliation. The Ru(0001) crystal is transferred back into the UHV chamber and subjected to a short heating step in order to allow surface analysis.

Figure 4 presents experimental results of the exfoliation of the silica bilayer from the Ru(0001) crystal (schematic in Figure 4a and b). The LEED pattern in Figure 4c exhibits both hexagonal reflexes that are characteristic for Ru(0001) and a ring feature that is typical for an amorphous silica bilayer. The amorphous network possesses short-range order due to its very regular SiO_4-tetrahedron building blocks. The building blocks exhibit characteristic pair nearest-neighbor (NN) distances but do not maintain any directional preference in their arrangement.[4] Therefore, a ring feature is observed in the diffraction pattern, which can be assigned to O−O NN distances. On the basis of the typical growth behavior of ultrathin silica films, the ring feature in LEED can be used for discerning between single layers and bilayers. Monolayer films on Ru(0001) and on Mo(112) are known to grow as crystalline films due to strong substrate influence.[16,36,37] The absence of a (2×2) refraction pattern characteristic for hexagonally ordered silica films therefore indicates a predominantly amorphous structure, which cannot be a monolayer film.[5,16] On the basis of the calibration of the deposited amount and the flatness evident from STM images, we conclude a bilayer structure.

In Figure 4d, only the hexagonal substrate reflexes are visible in LEED, taken after the exfoliation of the bilayer. Figure 4e and f show the change in morphology through STM. As seen in Figure 4e, the silica bilayer grows atomically flat on the substrate. Due to deposition of less than two full monolayers, round holes in the silica film of 4 to 9 nm in diameter reveal the underlying substrate. The preparation shown in Figure 4 has a coverage of 1.6 ± 0.1 ML. After exfoliation of the bilayer (Figure 4f), only bare terraces of the Ru(0001) with relatively straight step edges are visible in STM. Figure 4g presents AES data of the sample before and after the exfoliation procedure. The silica film produces silicon Auger peaks at 63 and 79 eV

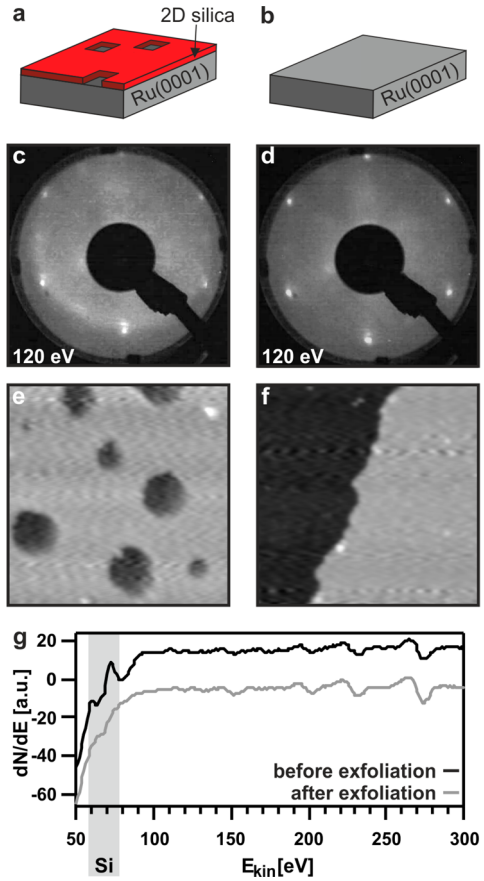

Figure 4. Exfoliation of silica bilayer from Ru(0001) substrate. (a) Schematic of silica bilayer supported on Ru(0001) and (b) Ru(0001) substrate after exfoliation. (c) LEED of silica bilayer supported on Ru(0001), showing hexagonal reflexes characteristic of Ru(0001) and a ring feature characteristic of the amorphous 2D silica film. (d) LEED of plain Ru(0001) substrate after exfoliation. (e) STM image of silica bilayer with 1.6 ± 0.1 ML coverage (50 nm × 50 nm, V_S = 1 V, I_T = 50 pA). (f) STM image of bare Ru(0001) surface after exfoliation (50 nm × 50 nm, V_S = 2 V, I_T = 50 pA). (g) AES spectra: silica bilayer supported on Ru(0001) (black curve) and plain Ru(0001) substrate after exfoliation (gray curve).

(black curve), which are not present anymore after the exfoliation procedure (gray curve). Substrate peaks are

DOI: 10.1021/acsnano.6b03929
ACS Nano 2016, 10, 7982−7989

observed before and after the exfoliation. LEED, AES, and STM measurements were taken on various positions on the surface. On the initial preparation, an even coverage of the substrate was thus established. After exfoliation, the complete sample surface was free of silica, indicating that the bilayer is lifted off entirely as one sheet.

The second step of the transfer consists in placing the PMMA-supported silica bilayer on a new substrate. In order to demonstrate the success of the bilayer transfer and to compare against the characteristics of the film pretransfer, we use LEED, AES, and STM. These techniques rely on electrons as probes and require flat, conducting substrates, ideally metal single crystals. Pt(111) lends itself as a natural choice for this proof-of-concept, since successful growth of a silica bilayer on Pt(111) has been shown before.[11] The PMMA-supported silica bilayer is placed on the platinum crystal, and a heat treatment in ambient is used to evaporate the PMMA, leaving the silica supported on platinum. Platinum has been observed to catalyze the decomposition of PMMA;[38] however, we expect the catalytic activity of a single-crystal surface to be negligible. Figure 5 presents data on a bare Pt(111) crystal (schematic 5a) and the transferred silica bilayer (schematic 5b). Figure 5c shows the LEED pattern of clean Pt(111), exhibiting hexagonal reflexes. After the transfer (Figure 5d), a ring in the LEED indicates the presence of a material that exhibits short-range order but no directionality. This is a very characteristic feature of the silica bilayer. A significant change in morphology can be seen in the STM, going from clean Pt(111) (Figure 5e) to silica on Pt(111) (Figure 5f). The film is atomically smooth and flat after the transfer procedure. Moreover, the characteristic open-hole appearance of the bilayer is completely preserved throughout the procedure, as the resemblance of the initial morphology (Figure 4e) and the transferred film (Figure 5f) is striking. From several STM images, the area of all round holes was analyzed, and an overall coverage of 1.6 ± 0.1 ML for the silica bilayer on Pt(111) determined, which agrees with the initial film coverage. The AES data in Figure 5g show typical Pt features before the transfer (blue curve). The spectrum taken after the transfer (red curve) exhibits an additional feature at 78 eV, indicating the presence of silicon. The low-energy peak for Si that was observed on Ru(0001) is concealed in this case by a Pt substrate peak at ~64 eV. An inset shows the oxygen feature at 508 eV, which is detected after the bilayer transfer. No residual carbon is observed in the spectrum, indicating successful PMMA removal through the heating treatment.

Figure 6 shows the transferred bilayer on Pt(111) at different length scales. Figure 6a is a photo of the entire sample, consisting of a round slab platinum single crystal, with a diameter of 9.2 mm. Figure 6b and c were obtained with ESEM, showing a uniform sample morphology at large ranges. The only parts of the sample exhibiting significantly differing textures were macroscopic defects, *e.g.*, scratches on the crystal. A higher resolution ESEM image in Figure 6c reveals holes of 20−30 nm in diameter. These features are also found in high-resolution STM images, like Figure 6d. Additional holes, smaller than 10 nm in diameter, are resolved in STM. Taken together, these images provide evidence for the structural preservation of the silica bilayer attained from the millimeter-scale exfoliation.

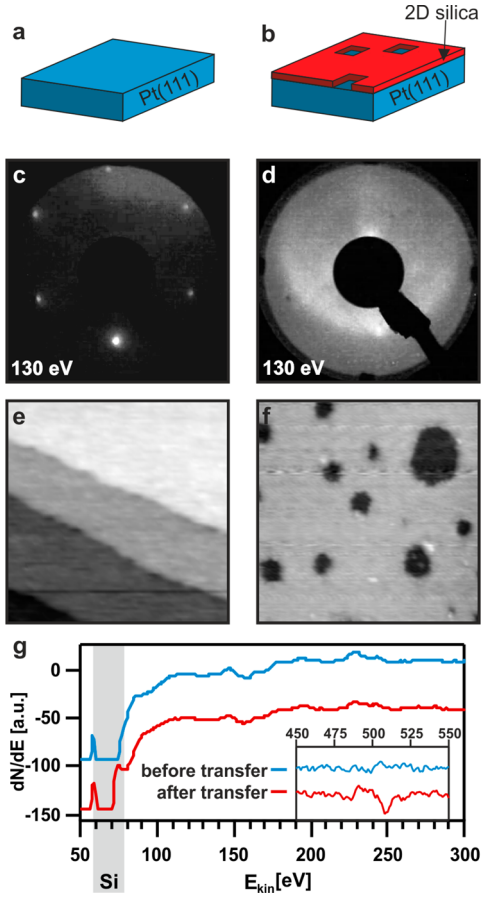

Figure 5. Transfer of silica bilayer to a Pt(111) substrate. (a) Schematic of bare Pt(111) substrate before transfer and (b) silica bilayer supported on Pt(111). (c) LEED of Pt(111) showing only reflexes of the hexagonal substrate before transfer. (d) LEED of silica bilayer supported on Pt(111). (e) STM image of bare Pt(111) surface (50 nm × 50 nm, V_S = 0.5 V, I_T = 50 pA). (f) STM image of silica bilayer on Pt(111) substrate with 1.6 ± 0.1 ML coverage (50 nm × 50 nm, V_S = 1 V, I_T = 100 pA). (g) AES spectra: Pt(111) substrate before transfer (blue curve, labeled "before transfer"); only the peaks characteristic for platinum are observed. Spectrum of silica bilayer supported on Pt(111) (red curve, labeled "after transfer") indicates the presence of silicon and oxygen.

DISCUSSION

Apparent Step Heights from STM Images. The comparison of STM images in Figures 4 and 5 reveals morphologies that are indicative for the presence of a silica bilayer (exhibiting round holes) or a plain metal surface (exhibiting straight step edges). Furthermore, changes in the apparent step heights correspond with the system changes, as shown in Figure 7. The STM images of silica on the growth and the target substrate as well as the bare substrates are shown on the left-hand side. A green line indicates the location of the respective line profile, given in the panels on the right-hand side. These values should be used with caution when true step heights are discussed, as the tunneling current is influenced by proximity of tip and sample, but also by local densities of states. Therefore, these parameters need to be carefully deconvoluted to gain true height information.[39,40] In the case of this study, we can use the line profiles to compare relative heights of the oxide film on the growth substrate *versus* the target substrate, which are both metallic and were scanned with the same metallic tip. On both substrates the silica bilayer exhibits holes with an apparent depth of 3 Å. This value significantly differs from the 2 Å step heights that are seen on Pt(111) and 4 Å double steps that are seen on Ru(0001).

DOI: 10.1021/acsnano.6b03929
ACS Nano 2016, 10, 7982−7989

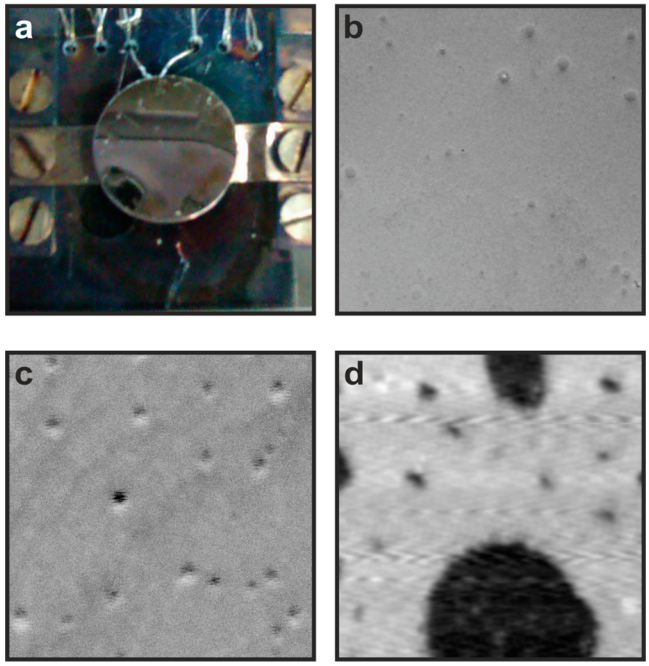

Figure 6. Silica bilayer on Pt(111) at different length scales. (a) Photo of Pt(111) single crystal mounted on sapphire holder; diameter of crystal slab is 9.2 mm. (b) ESEM image of silica bilayer, 500 μm × 500 μm, contrast inverted, showing even coverage (acceleration voltage H_A = 7.5 kV, p_{O2} = 20 Pa). (c) ESEM image of silica bilayer, 500 nm × 500 nm, contrast inverted, revealing large round holes with diameters of 20−40 nm (H_A = 12.5 kV, p_{O2} = 20 Pa). (d) STM image of silica bilayer (50 nm × 50 nm, V_S = 0.5 V, I_T = 100 pA), revealing open holes with diameters of 30 nm and smaller.

Quality of Film Transfer. A set of complementary techniques has been utilized to verify the successful transfer of the 2D silica film. The chemical signature from AES indicates that silica has been transferred to platinum. The characteristic ring feature in LEED shows that the transferred film possesses short-range order but no directional preference. The morphology found in STM is comparable for the silica bilayer before and after the transfer. STM also reveals holes that result from sub-bilayer coverage. The quantitative analysis of these holes yields a coverage value of 1.6 ± 0.1 ML for the film before and after the transfer. This agreement between initial and final coverage is evidence for a transfer method that preserves material integrity. Transferring ultrathin films often leads to mechanical damage, such as wrinkles or tears. As shown in Figure 6b, even on a 500 μm × 500 μm scan, such damage has not been observed. The investigation with ESEM reveals a smooth film covering the entire sample, without wrinkles, tears, or other obvious transfer-related damage. This indicates a remarkable stability of the ultrathin silica film. Furthermore, both the ruthenium and the platinum substrate are roughly 1 cm in diameter, and the transferred silica films correspond in size. We expect that this micromechanical cleavage approach can be performed in an analogous way on significantly larger sample surfaces, as well.

Film cleanliness is a further requirement of transferable 2D layers. We use mild heating for evaporating the transfer medium, followed by a short annealing step in the UHV chamber to clean the sample further. Longer annealing steps can also be implemented without affecting the silica bilayer.

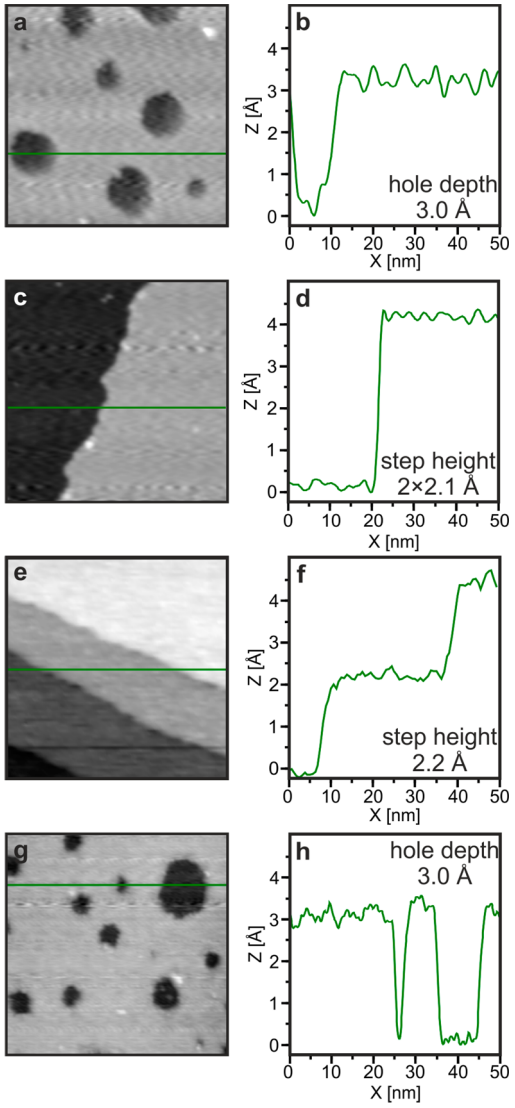

Figure 7. Apparent step heights measured with STM. (a, b) Silica bilayer on Ru(0001), hole depth 3 Å. (c, d) Plain Ru(0001) after exfoliation, characteristic double steps of 2 × 2.1 Å step height. (e, f) Bare Pt(111) surface, step height 2.2 Å. (g, h) Silica bilayer on Pt(111), hole depth 3 Å. All images in the left panel are 50 nm × 50 nm; STM scan parameters given in captions for Figures 4 and 5.

AES shows no carbon contamination of the samples, but may not provide sufficient signal intensities below one tenth of a monolayer. STM images indicate that the surface is free from adsorbates. Due to the high thermal and chemical stability of the 2D silica film, harsher cleaning treatments including solvent-based protocols should be applicable if needed.

The method presented here provides large-scale sheets of silica bilayers that possess 10−25% holes. These may be used as basic building blocks for assembling insulating layers with precise thickness control. Stacking two or more silica bilayers would result in a dielectric layer of tunable thickness without compromising flatness. Holes in one layer would thereby likely be covered by the next layer. Two stacked layers may be sufficiently thick to suppress electronic states of an underlying material extending into the vacuum, thereby providing an effective tunneling barrier.[26]

Exfoliation Method. The mechanical exfoliation method utilized in this study relies on a balance of adhesive forces. The

DOI: 10.1021/acsnano.6b03929
ACS Nano 2016, 10, 7982−7989

adhesion of the silica film on the metal substrate needs to be overcome by the adhesion between the polymer film and the silica film. Hence, it may be viewed as a variation on adhesive tape assisted exfoliation procedures ubiquitous in thin film technology, also known as micromechanical cleavage.[41] Note, however, that mechanical exfoliation using standard adhesive tape was not successful for this sample system. The silica film on Ru(0001) remained unaffected by adhesive tape treatment, as evident from unchanged LEED and AES measurements. This was surprising, as the adhesion energy of silica bilayers on ruthenium has been predicted to be very close to the interlayer adhesion of graphite layers,[1] which can be cleaved using adhesive tape.[41] The adhesion provided by a PMMA film applied *via* spin coating was sufficient to exfoliate the silica bilayer. Simply speaking, we assume that the success of mechanical cleavage depends on overcoming the threshold value of substrate adhesion.

Furthermore, the stiffness of the silica bilayer may also influence the success of exfoliation. A recent DFT study compares mechanical properties of silica bilayers with those of graphene, yielding different relative values for tensile and flexural bending stiffness.[28] Additional experimental studies are needed to shed light on the influence of these mechanical properties.

Perspective. The silica bilayer preparations used in this study possess certain structural features promoting transferability. The partial coverage resulting in round hole features is assumed to improve adhesion of the PMMA layer at these additional edge sites. Films of up to 1.8 ML coverage have been exfoliated successfully. Since mainly bilayers are formed, this corresponds to 10% of the surface area exposing the substrate and 90% of the surface covered with a bilayer.

Further studies are needed to understand whether the reason lies in stronger substrate adhesion of closed films or in improved friction of the PMMA on the partial coverage. On the basis of the successful proof-of-concept, we propose ways to shift the balance of adhesive forces in order to transfer films with higher coverage.

The atomic structure at coverages below 1.8 ML is predominantly amorphous, minimizing registry and attractive interaction with the substrate. A fully closed bilayer possesses larger crystalline domains in registry with the hexagonal ruthenium lattice, which may lead to a more efficient van der Waals interaction. Such bilayer films cannot be mechanically exfoliated by mere adhesion to a PMMA sheet.

It has been shown that the choice of the growth substrate is a way to tune the atomic structure of the silica layer. On Ru(0001) substrates, closed bilayer films typically exhibit predominantly crystalline structures,[42] which are assumed to adhere more strongly to the metal due to substrate registry. When Pt(111) is used as the growth substrate, only amorphous bilayer films have been observed.[11] Such a predominantly amorphous bilayer presumably interacts less effectively with the substrate, so that the adhesion may be overcome by the exfoliation method used in this study.

Another parameter is the choice of polymer used in the procedure. The additional edges exposed in the bilayer with partial coverage may improve the friction coefficient for the polymer-based exfoliation. Many polymers and adhesive tapes have been suggested for exfoliating thin films.[17] In this parameter space, another compound may be found that adheres to the silica bilayer system more strongly and can exfoliate a closed film from its growth substrate. Furthermore, an alternative method from the library of 2D exfoliation techniques, such as a substrate etching or bubbling route, may be developed to transfer the bilayer.[43,44]

CONCLUSION

In summary, a 2D silicon dioxide film has been transferred from the growth substrate to a new support. ESEM reveals that the majority of the new Pt support (diameter 9.2 mm) is covered with the silica bilayer. LEED and STM indicate preservation of the morphology and well-defined amorphous bilayer structure. Also, AES detects no carbon residue on the sample, indicating that the heat treatment is a very effective method for removing the organic polymer layer. A near-perfect transfer of the film highlights the robustness of this silica sheet, which is promising for future applications in nanotechnology.

METHODS

Techniques. The characterization of the freshly prepared films as well as the transferred films was performed in the same UHV setup. The chamber is equipped with LEED and AES optics (both performed with a 4-grid optics ErLEED by SPECS) and a low-temperature STM. LEED provides information on symmetry/order on the investigated surface, while AES is element-sensitive. Both techniques probe the sample surface in the micrometer range.

STM shows the sample morphology in real space and can achieve subnanometer lateral resolution. Technical details of the microscope sensor are provided in ref 45. For image smoothing and analysis, WSxM software was used.[46] Combined, all three techniques provide comprehensive information on the sample.

After transferring the silica bilayer to Pt(111) and subsequent characterization using LEED, AES, and low-temperature STM, the sample was also investigated with a FEI Quanta 200 environmental scanning electron microscopy. This microscope is equipped with a home-built heating stage and a gas-feeding system for imaging under controlled atmosphere at pressures of up to 2000 Pa. The sample was heated to around 300 °C, while an oxygen atmosphere of 20 Pa was provided to sustain a subsurface oxygen layer. This environment also prevents the formation of electron beam induced surface contaminations, which are a well-known problem in scanning electron microscopy (SEM).[47] They are caused by the interaction of the electron beam with residual gas molecules and the deposition of charged species at the place where the beam hits the sample. The contamination layer that is forming during imaging leads to attenuation of the secondary electron signal and a loss of structural sensitivity. Preventing the formation of this contamination layer is a big advantage of ESEM.

In the ESEM, the sample can be flexibly observed over a large range of magnifications, revealing structural information from the milli- to the micrometer scale and thus a better overview of sample coverage.

Preparation. Figure 1 shows a schematic of the transfer steps. In ultrahigh vacuum, a bilayer silica film was prepared on a Ru(0001) single crystal *via* physical vapor deposition and subsequent annealing (Figure 1a).[2] A film with 1.6 ML coverage was prepared, resulting in an atomically flat sheet of two layers thickness, exhibiting holes that reveal the metal substrate. We denote this coverage by 1.6 ML with respect to the bilayer structure of the film. In this convention, 1 ML refers to a monolayer film that is connected with Si−O−Ru bridges to the substrate, while 2 ML would denote a fully closed bilayer. By calibrating evaporator flux and deposition time, the coverage can be tuned precisely. A PMMA solution (20.7 wt %) was prepared by dissolving PMMA pellets (product name Polymethylmethacrylat Formmasse 7N, supplier Röhm GmbH, Darmstadt, Germany, now Evonik Industries AG) in acetone. The PMMA has an approximate molecular weight of 120 kDa.[48] The use of ultrasound to expedite the solvation is not recommended, since ultrasound leads to scission of polymer chains.[49] Under ambient conditions, the silica/Ru(0001) was spin-coated (Figure 1b) at approximately 1650 rpm with the PMMA solution (0.5 mL) and the PMMA film was mechanically cleaved after

DOI: 10.1021/acsnano.6b03929
ACS Nano 2016, 10, 7982−7989

a short drying time of roughly 3 min (Figure 1c). The resulting PMMA film supporting the silica bilayer (Figure 1d) is approximately 0.3 mm thick. In UHV, a Pt(111) single crystal was cleaned and a layer of oxygen was adsorbed on the crystal. Under ambient conditions, the PMMA film supporting the silica bilayer was placed on the Pt(111) single crystal, silica-side down (Figure 1e). By placing the sample on a heating plate at 300 °C for 3 h, the PMMA was evaporated completely. The result was a silica film supported on Pt(111) (Figure 1f). For analysis with LEED, AES, and STM, the plain Ru(0001) crystal after exfoliation and the transferred silica film/Pt(111) were placed in UHV again. Surface adsorbates were removed by a short heating step (860 °C for 5 min) in oxygen to facilitate analysis.

AUTHOR INFORMATION

Corresponding Author

*Phone (M. Heyde): +49 30 8413 4149. E-mail: heyde@fhi-berlin.mpg.de.

Notes

The authors declare no competing financial interest.

ACKNOWLEDGMENTS

The authors are grateful to Dr. Gerardo Algara-Siller for helpful discussions. C.B. is grateful to the CRC 1109, funded by the Deutsche Forschungsgemeinschaft, for financial support. K.M.B. gratefully acknowledges funding through the Alexander von Humboldt Foundation. Parts of this work have been used in a patent application filed with the European Patent Office (application number EP16158906.4).

REFERENCES

(1) Löffler, D.; Uhlrich, J. J.; Baron, M.; Yang, B.; Yu, X.; Lichtenstein, L.; Heinke, L.; Büchner, C.; Heyde, M.; Shaikhutdinov, S.; Freund, H.-J.; Włodarczyk, R.; Sierka, M.; Sauer, J. Growth and Structure of Crystalline Silica Sheet on Ru(0001). *Phys. Rev. Lett.* **2010**, *105*, 1−4.

(2) Lichtenstein, L.; Büchner, C.; Yang, B.; Shaikhutdinov, S.; Heyde, M.; Sierka, M.; Włodarczyk, R.; Sauer, J.; Freund, H.-J. The Atomic Structure of a Metal-Supported Vitreous Thin Silica Film. *Angew. Chem., Int. Ed.* **2012**, *51*, 404−407.

(3) Lichtenstein, L.; Heyde, M.; Freund, H.-J. Crystalline-Vitreous Interface in Two Dimensional Silica. *Phys. Rev. Lett.* **2012**, *109*, 1−5.

(4) Lichtenstein, L.; Heyde, M.; Freund, H.-J. Atomic Arrangement in Two-Dimensional Silica: From Crystalline to Vitreous Structures. *J. Phys. Chem. C* **2012**, *116*, 20426−20432.

(5) Büchner, C.; Lichtenstein, L.; Yu, X.; Boscoboinik, J. A.; Yang, B.; Kaden, W. E.; Heyde, M.; Shaikhutdinov, S. K.; Włodarczyk, R.; Sierka, M.; Sauer, J.; Freund, H.-J. Ultrathin Silica Films: The Atomic Structure of Two-Dimensional Crystals and Glasses. *Chem. - Eur. J.* **2014**, *20*, 9176−9183.

(6) Lichtenstein, L.; Heyde, M.; Ulrich, S.; Nilius, N.; Freund, H.-J. Probing the Properties of Metal−oxide Interfaces: Silica Films on Mo and Ru Supports. *J. Phys.: Condens. Matter* **2012**, *24*, 354010.

(7) Büchner, C.; Lichtenstein, L.; Stuckenholz, S.; Heyde, M.; Ringleb, F.; Sterrer, M.; Kaden, W. E.; Giordano, L.; Pacchioni, G.; Freund, H. Adsorption of Au and Pd on Ruthenium-Supported Bilayer Silica. *J. Phys. Chem. C* **2014**, *118*, 20959−20969.

(8) Yu, X.; Emmez, E.; Pan, Q.; Yang, B.; Pomp, S.; Kaden, W. E.; Sterrer, M.; Shaikhutdinov, S.; Freund, H.-J.; Goikoetxea, I.; Wlodarczyk, R.; Sauer, J. Electron Stimulated Hydroxylation of a Metal Supported Silicate Film. *Phys. Chem. Chem. Phys.* **2016**, *18*, 3755−3764.

(9) Emmez, E.; Yang, B.; Shaikhutdinov, S.; Freund, H.-J. Permeation of a Single-Layer SiO2Membrane and Chemistry in Confined Space. *J. Phys. Chem. C* **2014**, *118*, 29034−29042.

(10) Schroeder, T.; Adelt, M.; Richter, B.; Naschitzki, M.; Bäumer, M.; Freund, H.-J. Epitaxial Growth of SiO2 on Mo(112). *Surf. Rev. Lett.* **2000**, *7*, 7−14.

(11) Yu, X.; Yang, B.; Boscoboinik, J. A.; Shaikhutdinov, S.; Freund, H.-J. Support Effects on the Atomic Structure of Ultrathin Silica Films on Metals. *Appl. Phys. Lett.* **2012**, *100*, 1−4.

(12) Altman, E. I.; Götzen, J.; Samudrala, N.; Schwarz, U. D. Growth and Characterization of Crystalline Silica Films on Pd (100). *J. Phys. Chem. C* **2013**, *117*, 26144−26155.

(13) Ben Romdhane, F.; Björkman, T.; Rodríguez-Manzo, J. A.; Cretu, O.; Krasheninnikov, A. V.; Banhart, F. *In Situ* Growth of Cellular Two-Dimensional Silicon Oxide on Metal Substrates. *ACS Nano* **2013**, *7*, 5175−5180.

(14) Huang, P. Y.; Kurasch, S.; Srivastava, A.; Skakalova, V.; Kotakoski, J.; Krasheninnikov, A. V.; Hovden, R.; Mao, Q.; Meyer, J. C.; Smet, J.; Muller, D. A.; Kaiser, U. Direct Imaging of a Two-Dimensional Silica Glass on Graphene. *Nano Lett.* **2012**, *12*, 1081−1086.

(15) Yu, X.; Yang, B.; Anibal Boscoboinik, J.; Shaikhutdinov, S.; Freund, H.-J. Support Effects on the Atomic Structure of Ultrathin Silica Films on Metals. *Appl. Phys. Lett.* **2012**, *100*, 151608.

(16) Yang, B.; Kaden, W. E.; Yu, X.; Boscoboinik, J. A.; Martynova, Y.; Lichtenstein, L.; Heyde, M.; Sterrer, M.; Włodarczyk, R.; Sierka, M.; Sauer, J.; Shaikhutdinov, S.; Freund, H.-J. Thin Silica Films on Ru(0001): Monolayer, Bilayer and Three-Dimensional Networks of [SiO4] Tetrahedra. *Phys. Chem. Chem. Phys.* **2012**, *14*, 11344−11351.

(17) Ferrari, A. C.; Bonaccorso, F.; Falko, V.; Novoselov, K. S.; Roche, S.; Bøggild, P.; Borini, S.; Koppens, F.; Palermo, V.; Pugno, N.; Garrido, J. A.; Sordan, R.; Bianco, A.; Ballerini, L.; Prato, M.; Lidorikis, E.; Kivioja, J.; Marinelli, C.; Ryhänen, T.; Morpurgo, A.; et al. Science and Technology Roadmap for Graphene, Related Two-Dimensional Crystals, and Hybrid Systems. *Nanoscale* **2015**, *7*, 4598−4810.

(18) Osada, M.; Sasaki, T. Two-Dimensional Dielectric Nanosheets: Novel Nanoelectronics From Nanocrystal Building Blocks. *Adv. Mater.* **2012**, *24*, 210−228.

(19) Gao, G.; Gao, W.; Cannuccia, E.; Taha-Tijerina, J.; Balicas, L.; Mathkar, A.; Narayanan, T. N.; Liu, Z.; Gupta, B. K.; Peng, J.; Yin, Y.; Rubio, A.; Ajayan, P. M. Artificially Stacked Atomic Layers: Toward New van Der Waals Solids. *Nano Lett.* **2012**, *12*, 3518−3525.

(20) Cullen, W. G.; Yamamoto, M.; Burson, K. M.; Chen, J. H.; Jang, C.; Li, L.; Fuhrer, M. S.; Williams, E. D. High-Fidelity Conformation of Graphene to SiO2 Topographic Features. *Phys. Rev. Lett.* **2010**, *105*, 1−4.

(21) Rudenko, A. N.; Keil, F. J.; Katsnelson, M. I.; Lichtenstein, A. I. Interfacial Interactions between Local Defects in Amorphous SiO2 and Supported Graphene. *Phys. Rev. B: Condens. Matter Mater. Phys.* **2011**, *84*, 1−9.

(22) Ishigami, M.; Chen, J. H.; Cullen, W. G.; Fuhrer, M. S.; Williams, E. D. Atomic Structure of Graphene on SiO2. *Nano Lett.* **2007**, *7*, 1643−1648.

(23) Dean, C. R.; Young, A. F.; Meric, I.; Lee, C.; Wang, L.; Sorgenfrei, S.; Watanabe, K.; Taniguchi, T.; Kim, P.; Shepard, K. L.; Hone, J. Boron Nitride Substrates for High-Quality Graphene Electronics. *Nat. Nanotechnol.* **2010**, *5*, 722−726.

(24) Hwang, E. H.; Adam, S.; Sarma, S. D. Carrier Transport in Two-Dimensional Graphene Layers. *Phys. Rev. Lett.* **2007**, *98*, 186806.

(25) Katsnelson, M.; Geim, A. Electron Scattering on Microscopic Corrugations in Graphene. *Philos. Trans. R. Soc., A* **2008**, *366*, 195−204.

(26) Muller, D. A.; Sorsch, T.; Moccio, S.; Baumann, F. H.; Evans-Lutterodt, K.; Timp, G. The Electronic Structure at the Atomic Scale of Ultrathin Gate Oxides. *Nature* **1999**, *399*, 758−761.

(27) Larciprete, R.; Lacovig, P.; Orlando, F.; Dalmiglio, M.; Omiciuolo, L.; Baraldi, A.; Lizzit, S. Chemical Gating of Epitaxial Graphene through Ultrathin Oxide Layers. *Nanoscale* **2015**, *7*, 12650−12658.

(28) Gao, E.; Xie, B.; Xu, Z. Two-Dimensional Silica: Structural, Mechanical Properties, and Strain-Induced Band Gap Tuning. *J. Appl. Phys.* **2016**, *119*, 1−7.

(29) Chen, Z.-G.; Zou, J.; Liu, G.; Li, F.; Wang, Y.; Wang, L.; Yuan, X.-L.; Sekiguchi, T.; Cheng, H.-M.; Lu, G. Q. Novel Boron Nitride Hollow Nanoribbons. *ACS Nano* **2008**, *2*, 2183−2191.

DOI: 10.1021/acsnano.6b03929
ACS Nano 2016, 10, 7982−7989

(30) Watanabe, K.; Taniguchi, T.; Kanda, H. Direct-Bandgap Properties and Evidence for Ultraviolet Lasing of Hexagonal Boron Nitride Single Crystal. *Nat. Mater.* **2004**, *3*, 404−409.
(31) Blase, X.; Rubio, A.; Louie, S. G.; Cohen, M. L. Stability and Band Gap Constancy of Boron Nitride Nanotubes. *Europhys. Lett.* **1994**, *28*, 335−340.
(32) Yang, B.; Kaden, W. E.; Emmez, E.; Yu, X.; Boscoboinik, J. A.; Sterrer, M.; Shaikhutdinov, S.; Freund, H.-J. Hydroxylation of Metal Supported Sheet-Like Silica Films. *J. Phys. Chem. C* **2013**, *117*, 8336.
(33) Schlexer, P.; Giordano, L.; Pacchioni, G. Adsorption of Li, Na, K, and Mg Atoms on Amorphous and Crystalline Silica Bilayers on Ru(0001): A DFT Study. *J. Phys. Chem. C* **2014**, *118*, 15884−15897.
(34) Schlexer, P.; Pacchioni, G.; Włodarczyk, R.; Sauer, J. CO Adsorption on a Silica Bilayer Supported on Ru(0001). *Surf. Sci.* **2016**, *648*, 2−9.
(35) Büchner, C.; Schlexer, P.; Lichtenstein, L.; Stuckenholz, S.; Heyde, M.; Freund, H.-J. Topological Investigation of Two-Dimensional Amorphous Materials. *Z. Phys. Chem.* **2014**, *228*, 587−607.
(36) Weissenrieder, J.; Kaya, S.; Lu, J.-L.; Gao, H.-J.; Shaikhutdinov, S.; Freund, H.-J.; Sierka, M.; Todorova, T.; Sauer, J. Atomic Structure of a Thin Silica Film on a Mo(112) Substrate: A Two-Dimensional Network of SiO4 Tetrahedra. *Phys. Rev. Lett.* **2005**, *95*, 076103.
(37) Mathur, S.; Vlaic, S.; Machado-Charry, E.; Vu, A. D.; Guisset, V.; David, P.; Hadji, E.; Pochet, P.; Coraux, J. Degenerate Epitaxy-Driven Defects in Monolayer Silicon Oxide on Ruthenium. *Phys. Rev. B: Condens. Matter Mater. Phys.* **2015**, *92*, 2−6.
(38) Longchamp, J.-N.; Escher, C.; Fink, H.-W. Ultraclean Freestanding Graphene by Platinum-Metal Catalysis. *J. Vac. Sci. Technol. B* **2013**, *31*, 1−3.
(39) Jałochowski, M.; Palotás, K.; Krawiec, M. Spilling of Electronic States in Pb Quantum Wells. *Phys. Rev. B: Condens. Matter Mater. Phys.* **2016**, *93*, 035437.
(40) Højrup Hansen, K.; Worren, T.; Lægsgaard, E.; Besenbacher, F.; Stensgaard, I. Bias Dependent Apparent Height of an Al2O3 Thin Film on NiAl(110), and of Supported Pd Clusters. *Surf. Sci.* **2001**, *475*, 96−102.
(41) Güntherodt, H.-J.; Wiesendanger, R. In *Scanning Tunneling Microscopy I*, 2nd ed.; Güntherodt, H.-J.; Wiesendanger, R., Eds.; Springer-Verlag: Berlin Heidelberg, 1994.
(42) Lichtenstein, L. *The Structure of Two-Dimensional Vitreous Silica*; Freie Universität: Berlin, 2012.
(43) Reina, A.; Son, H.; Jiao, L.; Fan, B.; Dresselhaus, M. S.; Liu, Z.; Kong, J. Transferring and Identification of Single- and Few-Layer Graphene on Arbitrary Substrates. *J. Phys. Chem. C* **2008**, *112*, 17741−17744.
(44) Li, X.; Cai, W.; An, J.; Kim, S.; Nah, J.; Yang, D.; Piner, R.; Velamakanni, A.; Jung, I.; Tutuc, E.; Banerjee, S. K.; Colombo, L.; Ruoff, R. S. Large-Area Synthesis of High-Quality and Uniform Graphene Films on Copper Foils. *Science* **2009**, *324*, 1312−1314.
(45) Heyde, M.; Simon, G. H.; Rust, H.-P.; Freund, H.-J. Probing Adsorption Sites on Thin Oxide Films by Dynamic Force Microscopy. *Appl. Phys. Lett.* **2006**, *89*, 263107.
(46) Horcas, I.; Fernández, R.; Gómez-Rodríguez, J. M.; Colchero, J.; Gómez-Herrero, J.; Baro, A. M. WSXM: A Software for Scanning Probe Microscopy and a Tool for Nanotechnology. *Rev. Sci. Instrum.* **2007**, *78*, 1−8.
(47) Reimer, L. *Scanning Electron Microscopy*; Springer-Verlag: Berlin Heidelberg, 1998.
(48) Cappella, B.; Sturm, H.; Weidner, S. M. Breaking Polymer Chains by Dynamic Plowing Lithography. *Polymer* **2002**, *43*, 4461−4466.
(49) Kemmere, M. F.; Kuijpers, M. W. A.; Keurentjes, J. T. F. Reaction Calorimetry for the Development of Ultrasound-Induced Polymerization Processes in CO2-Expanded Fluids. *Macromol. Symp.* **2007**, *248*, 182−188.

DOI: 10.1021/acsnano.6b03929
ACS Nano 2016, 10, 7982−7989